

## Crossover between Weak Antilocalization and Weak Localization in a Magnetically Doped Topological Insulator

Minhao Liu,<sup>1</sup> Jinsong Zhang,<sup>1</sup> Cui-Zu Chang,<sup>1,2</sup> Zuocheng Zhang,<sup>1</sup> Xiao Feng,<sup>2</sup> Kang Li,<sup>2</sup> Ke He,<sup>2,\*</sup> Li-li Wang,<sup>2</sup> Xi Chen,<sup>1</sup> Xi Dai,<sup>2</sup> Zhong Fang,<sup>2</sup> Qi-Kun Xue,<sup>1,2</sup> Xucun Ma,<sup>2</sup> and Yayu Wang<sup>1,†</sup>

<sup>1</sup>State Key Laboratory of Low Dimensional Quantum Physics, Department of Physics, Tsinghua University, Beijing 100084, People's Republic of China

<sup>2</sup>Institute of Physics, Chinese Academy of Sciences, Beijing 100190, People's Republic of China

(Received 21 July 2011; published 19 January 2012)

We report transport studies on magnetically doped Bi<sub>2</sub>Se<sub>3</sub> topological insulator ultrathin films grown by molecular beam epitaxy. The magnetotransport behavior exhibits a systematic crossover between weak antilocalization and weak localization with the change of magnetic impurity concentration, temperature, and magnetic field. We show that the localization property is closely related to the magnetization of the sample, and the complex crossover is due to the transformation of Bi<sub>2</sub>Se<sub>3</sub> from a topological insulator to a topologically trivial dilute magnetic semiconductor driven by magnetic impurities. This work demonstrates an effective way to manipulate the quantum transport properties of the topological insulators by breaking time-reversal symmetry.

DOI: 10.1103/PhysRevLett.108.036805

PACS numbers: 73.20.Fz, 73.20.At, 73.21.-b, 73.50.-h

Topological insulators (TI) are a new class of quantum materials with an insulating bulk enclosed by topologically protected metallic boundaries [1–3]. The topological surface states of the three-dimensional (3D) TIs have a spin helical massless Dirac structure [4–6], and are robust against time-reversal invariant perturbations. This extraordinary property is notably exemplified by the absence of backscattering by nonmagnetic impurities [7–9] and the weak antilocalization (WAL) of the Dirac fermions [10–13]. Breaking the time-reversal symmetry (TRS) in the TIs is predicted to create a variety of exotic topological effects including the half-quantized Hall conductance [14], image magnetic monopoles [15], neutral Majorana fermions [16], giant magneto-optical effects [17], and quantized anomalous Hall effect [18]. Searching for these novel phenomena in magnetically doped TIs represents one of the most exciting areas in this field.

Magnetic doping of Bi<sub>2</sub>Se<sub>3</sub> has attracted particular attention because Bi<sub>2</sub>Se<sub>3</sub> is an ideal 3D TI with a large bulk energy gap and a Dirac point located outside the bulk bands [19,20]. On the surface of magnetically doped Bi<sub>2</sub>Se<sub>3</sub> single crystals, angle-resolved photoemission spectroscopy (ARPES) has revealed the opening of an energy gap at the Dirac point [21] and the creation of an odd multiples of Dirac fermions [22], both owing to the breaking of TRS by magnetic impurities. The transport properties of magnetically doped TIs, however, have not been investigated in a systematic manner despite their direct relevance to the topological magnetoelectric effects and spintronic device applications. In this Letter we report transport studies on Chromium (Cr) doped Bi<sub>2</sub>Se<sub>3</sub> ultrathin films grown by molecular beam epitaxy (MBE). With increasing Cr content, the low temperature magneto conductivity exhibits a systematic crossover from WAL to weak localization

(WL). In the high Cr regime where WL dominates at the ground state, WAL reenters as temperature rises but can be driven back to WL by strong magnetic field. By combining the transport and ARPES results, we propose that the complex crossover phenomena demonstrate the transformation of Bi<sub>2</sub>Se<sub>3</sub> from a TI to a topologically trivial dilute magnetic semiconductor (DMS) driven by magnetic impurities.

The Cr doped Bi<sub>2</sub>Se<sub>3</sub> (Bi<sub>2-x</sub>Cr<sub>x</sub>Se<sub>3</sub>) ultrathin films studied here are grown on sapphire (0001) substrate by MBE. The Cr dopants are evaporated simultaneously with the Bi and Se atoms and the concentration  $x$  is controlled by the evaporation temperature of the Knudsen cell containing the Cr source. The  $x$  value is determined by an atomic emission spectrometer on 100 quintuple layer (QL) thick Bi<sub>2-x</sub>Cr<sub>x</sub>Se<sub>3</sub> films grown under the same conditions. Transport properties are measured by standard four-probe ac lock-in method on devices schematically shown in Fig. 1(a), which is the same as that used in a previous report [11]. The thickness of the films is kept at 3QL because in this ultrathin regime the surface states play a major role in electrical transport due to the large surface to volume ratio [11,12] (the effect of film thickness is discussed in the supplementary materials [23]). ARPES measurements are performed *in situ* at  $T \sim 100$  K by using a Scienta SES-2002 analyzer.

Figure 1(b) shows the sheet resistance ( $R_{\square}$ ) vs temperature ( $T$ ) for a pure Bi<sub>2</sub>Se<sub>3</sub> and four Cr doped Bi<sub>2-x</sub>Cr<sub>x</sub>Se<sub>3</sub> films with  $x = 0.04, 0.07, 0.13,$  and  $0.23$ , respectively. All the  $R_{\square} - T$  curves show metallic behavior (positive slope) at high  $T$  and insulating behavior (divergent increase) at low  $T$ . The insulating tendency is enhanced progressively by Cr doping, indicating the suppression of electrical conductivity by magnetic impurities. Figure 1(c) shows that

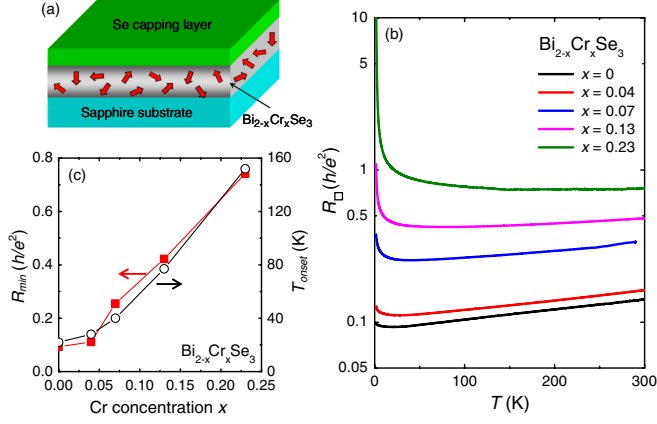


FIG. 1 (color online). (a) Schematic structure of the 3QL  $\text{Bi}_{2-x}\text{Cr}_x\text{Se}_3$  film on sapphire for transport studies. The thickness is not to scale. (b) The  $R_{\square} - T$  curves of the five  $\text{Bi}_{2-x}\text{Cr}_x\text{Se}_3$  films all show metallic behavior at high  $T$  but becomes insulating at low  $T$ . (c) Both the minimum resistance value ( $R_{\min}$ ) and the onset temperature ( $T_{\text{onset}}$ ) for the insulating behavior increases with  $x$ .

both the minimum resistance value and the onset temperature for the insulating behavior increase with  $x$ . The detrimental effect of magnetic doping is more dramatic at low  $T$ , where the resistance of the  $x = 0.23$  film is enhanced by more than 2 orders of magnitude from that of pure  $\text{Bi}_2\text{Se}_3$ . Both the  $R_{\square}$  vs  $T$  behavior and the doping dependence of  $T_{\text{onset}}$  suggest that the Kondo effect does not play a major

role in the observed phenomena, as discussed in detail in the supplementary materials [23].

Figures 2(a)–2(e) display the variation of Hall resistance ( $R_{yx}$ ) with magnetic field ( $H$ ) for the five  $\text{Bi}_{2-x}\text{Cr}_x\text{Se}_3$  films. The negative  $R_{yx}$  in all samples indicates that the Fermi energy ( $E_F$ ) always lies above the Dirac point, consistent with the ARPES results shown in Fig. 4. For pure  $\text{Bi}_2\text{Se}_3$  [Fig. 2(a)], the  $R_{yx}$  measured at  $T = 1.5$  K has a linear field dependence up to 5 T, as expected for nonmagnetic conductors. For the Cr doped films, the low  $T$  Hall traces start to develop a curvature. The nonlinearity becomes more pronounced as  $x$  increases, apparently due to the larger concentration of magnetic impurities. The overall pattern of the Hall curves in the heavily doped  $x = 0.23$  sample [Fig. 2(e)] resembles the anomalous Hall effect in DMS, where the total Hall resistance can be expressed as  $R_{yx} = R_A M(T, H) + R_N H$ .

Here  $R_A$  is the anomalous Hall coefficient,  $M(T, H)$  is the magnetization of the sample, and  $R_N$  is the normal Hall coefficient. There is no hysteresis in the magneto transport properties, indicating the absence of long-range ferromagnetic ordering. Nevertheless, the magnitude of the anomalous Hall term can be estimated by the intercept  $R_{yx}^0$  obtained by extrapolating the high field linear Hall curve to zero field, as indicated by the broken line in Fig. 2(e). The solid squares in Fig. 3(a) are the  $R_{yx}^0$  values of the five  $\text{Bi}_{2-x}\text{Cr}_x\text{Se}_3$  films measured at  $T = 1.5$  K, which increase systematically with  $x$ . The solid squares in Fig. 3(b) show

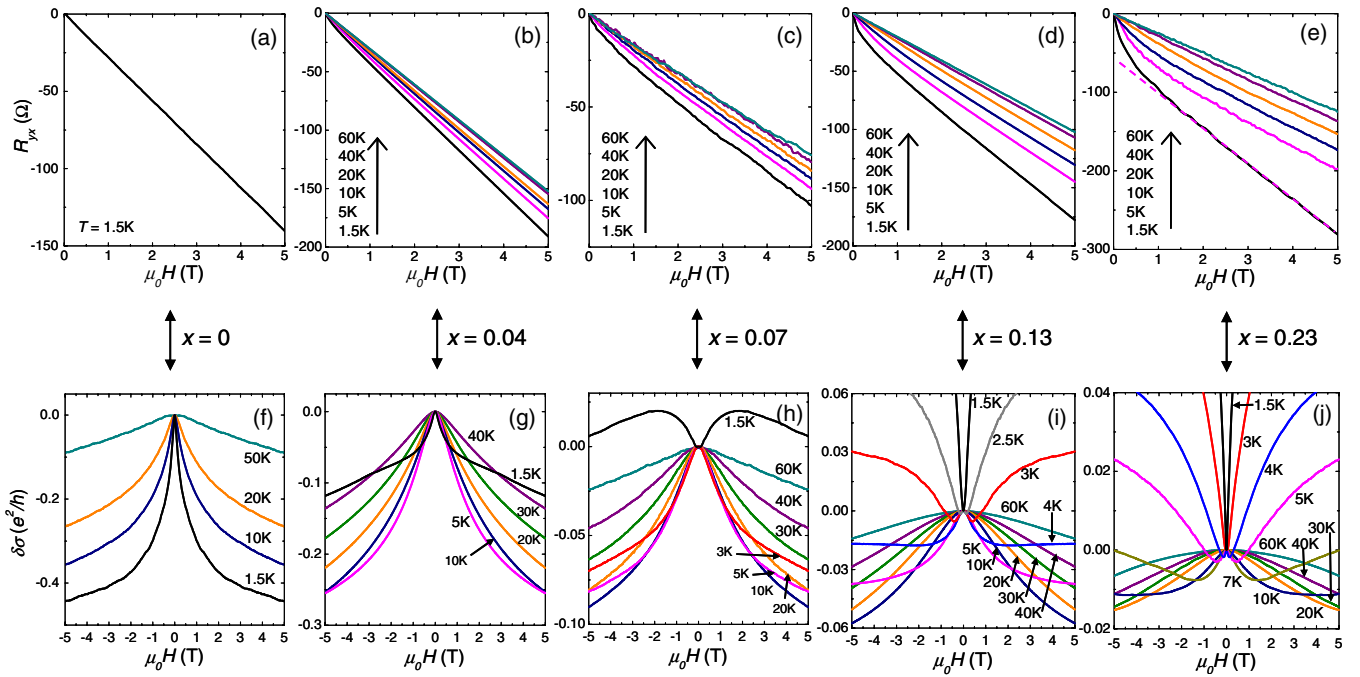


FIG. 2 (color online). (a) Pure  $\text{Bi}_2\text{Se}_3$  film shows linear Hall effect up to 5 T. (b) to (e) Hall traces in Cr doped  $\text{Bi}_{2-x}\text{Cr}_x\text{Se}_3$  films show more pronounced nonlinearity with increasing  $x$ . (f) and (g) Pure  $\text{Bi}_2\text{Se}_3$  and the  $x = 0.04$  films show negative MC characteristic of WAL. (h) The  $x = 0.07$  film shows a nonmonotonic MC at  $T = 1.5$  K and WAL at higher  $T$ . (i) and (j) The  $x = 0.13$  and  $x = 0.23$  films show sharp WL-like MC at  $T = 1.5$  K. At higher  $T$ , WAL dominates at low  $H$  while WL is recovered at high  $H$ .

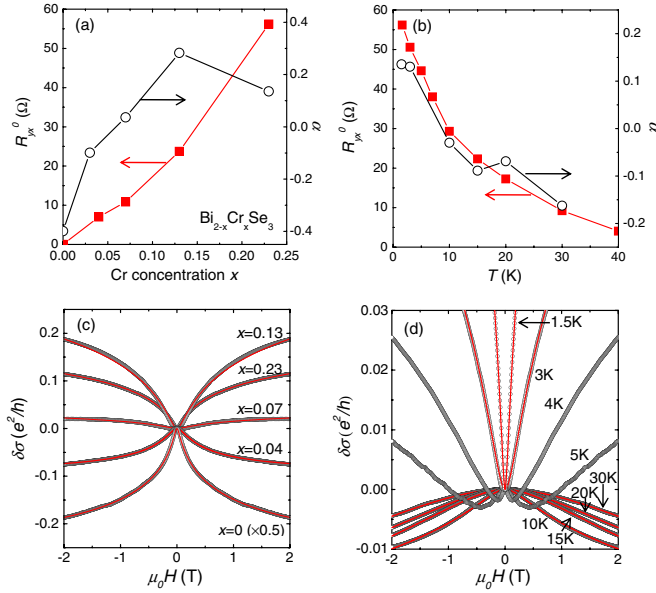


FIG. 3 (color online). (a) Red solid squares show the  $T = 1.5$  K  $R_{yx}^0$  as a function of  $x$ . Black open circles show the  $\alpha$  values in the HLN fit. (b) Red solid squares show  $T$ -dependent  $R_{yx}^0$  for the  $x = 0.23$  film. Black open circles show the  $\alpha$  values. (c) Black symbols are the  $T = 1.5$  K MC for all five  $\text{Bi}_{2-x}\text{Cr}_x\text{Se}_3$  films showing the crossover from WAL to WL. Red lines are the fits using the HLN formula. (d) Black symbols show the MC curves at representative  $T$  for the  $x = 0.23$  film and red curves are HLN fits at the low  $T$  and high  $T$  limits.

that the  $R_{yx}^0$  values of the heavily doped  $x = 0.23$  sample decrease systematically with increasing  $T$ .

Figures 2(f)–2(j) display the magnetoconductivity (MC)  $\delta\sigma(B) = \sigma(B) - \sigma(0)$  of the five  $\text{Bi}_{2-x}\text{Cr}_x\text{Se}_3$  films measured at varied temperatures. For pure  $\text{Bi}_2\text{Se}_3$  [Fig. 2(f)], the low field MC curves show sharp negative cusps characteristic of WAL, which has been observed in various TIs [10–13]. The WAL behavior can originate from strong spin-orbit-coupling (SOC) in the bulk and spin-momentum locking in the topological surface states [24]. In the ultra-thin MBE-grown TI film it has been shown that the WAL comes mainly from the surface states [12], in which the Dirac fermions travelling along two time-reversed self-crossing loops accumulate a  $\pi$  Berry phase. The destructive quantum interference between them reduces the return probability of the Dirac fermions, leading to a quantum enhancement to the classical Drude conductivity. WAL is suppressed by a perpendicular magnetic field, resulting in a negative MC as shown in Fig. 2(f). With the introduction of magnetic impurities, the localization behavior of the TIs is significantly altered. For the lightly doped  $x = 0.04$  sample [Fig. 2(g)], MC is still negative, but the low field cusp is not as sharp as that measured at the same  $T$  in pure  $\text{Bi}_2\text{Se}_3$ , indicating weakened WAL effect. In the intermediately doped  $x = 0.07$  sample [Fig. 2(h)], a qualitatively new feature emerges. For the  $T = 1.5$  K curve, MC remains small and negative up to  $\mu_0 H \sim 0.2$  T. It becomes positive

above that, reaches a peak at 2 T, and then starts to decrease at even higher field. The nonmonotonic behavior disappears as  $T$  is warmed to 3 K, when MC becomes negative again like that in the less doped samples. When the doping level reaches  $x = 0.13$  [Fig. 2(i)], the  $T = 1.5$  K curve shows a sharp positive cusp at low field, in stark contrast to the WAL. This is characteristic of the commonly observed WL, which is due to the constructive quantum interference between the two loops. However, as  $T$  is warmed slightly to 2 K, the low field MC recovers the negative WAL behavior, although it bends over to WL again at higher field. The WL behavior becomes more dominant in the heavily doped  $x = 0.23$  sample [Fig. 2(j)]. Here the WL cusp is extremely sharp at  $T = 1.5$  K and persists to  $T = 3$  K. At higher  $T$  the crossover to WAL occurs but WL is recovered at significantly lower fields than in the  $x = 0.13$  sample, indicating much stronger tendency towards WL.

The black symbols in Fig. 3(c) summarize the  $\delta\sigma(B)$  curves for the five  $\text{Bi}_{2-x}\text{Cr}_x\text{Se}_3$  films measured at  $T = 1.5$  K, which reveal a systematic evolution from typical WAL in  $x = 0$  to typical WL in  $x = 0.23$ . The black symbols in Fig. 3(d) are several representative MC curves in the  $x = 0.23$  film to highlight the peculiar WL to WAL crossover driven by temperature and magnetic field. Although the patterns shown here are quite rich and complex, the general trend is very clear: WL becomes more pronounced in the regime of high magnetic impurity level, low temperature, and strong magnetic field. Taken collectively, all these factors are favorable for enhancing the field-induced magnetization of the sample. Therefore WL seems to be intimately related to magnetization, hence the degree of TRS breaking.

We next turn to a more quantitative analysis of the WAL to WL crossover phenomena. The effect of localization on the two-dimensional (2D) MC can be described by the Hikami-Larkin-Nagaoka (HLN) theory [25]. In the low mobility regime, the weak field conductance variation is

$$\begin{aligned} \delta\sigma(B) &= \sigma(B) - \sigma(0) \\ &= \frac{\alpha e^2}{2\pi^2\hbar} \left[ \psi\left(\frac{1}{2} + \frac{\hbar}{4eBl_\phi^2}\right) - \ln\left(\frac{\hbar}{4eBl_\phi^2}\right) \right]. \end{aligned} \quad (1)$$

Here,  $l_\phi$  is the phase coherence length,  $\psi$  is the digamma function, and  $\alpha$  is a coefficient indicating the type of localization. We first apply the HLN formula to the MC curves of the five  $\text{Bi}_{2-x}\text{Cr}_x\text{Se}_3$  films measured at  $T = 1.5$  K, as shown by the red curves in Fig. 3(c). The MC of pure  $\text{Bi}_2\text{Se}_3$  can be fit very well by Eq. (1) with  $\alpha = -0.40$ , consistent with typical WAL behavior. In the heavily doped  $x = 0.23$  sample, Eq. (1) gives excellent fit to the MC curve with  $\alpha = 0.14$ , indicating typical WL behavior. For the intermediately doped samples, the data can still be described fairly well by the HLN formula, although the fit is less satisfactory at weak fields. The open circles in

Fig. 3(a) summarize the evolution of  $\alpha$  with the magnetic impurity level. The sign changes from negative to positive near  $x = 0.07$ , indicating a smooth crossover from WAL to WL with increasing magnetic impurity level. The roughly similar trend between  $\alpha$  and  $R_{yx}^0$  reveals the close relationship between the magnetization and localization. The drop of  $\alpha$  in the  $x = 0.23$  sample may be due to the strongly reduced quantum interference effect when the magnetic impurity level becomes too high.

The temperature evolution of MC in the  $x = 0.23$  sample [Fig. 3(d)] is more complex for a quantitative analysis. We find that at the low  $T$  (high  $T$ ) limit the curves can be fit well by Eq. (1) using positive (negative)  $\alpha$ , indicating typical WL (WAL) behavior. The  $T$  dependence of  $\alpha$  also roughly follows  $R_{yx}^0$  [Fig. 3(b)], again demonstrating the close relationship between magnetization and localization. In the intermediate  $T$  range ( $3 \text{ K} < T < 10 \text{ K}$ ), however, the highly nonmonotonic MC curves cannot be described by the HLN formula. We suspect that in this regime a model with two competing terms is needed. Details about the data analysis can be found in the supplementary materials [23].

What is the physical mechanism that underlies the complex WAL to WL crossover? Recently it has been proposed that due to the TRS-breaking gap opened at the Dirac point of the topological surface states, magnetically doped TIs will undergo a WAL to WL crossover in a very similar manner to that shown in Fig. 3(c) [26]. Although this picture may be highly relevant to the observed crossover behavior, our ARPES results present a more complicated scenario. In  $\text{Bi}_{2-x}\text{Cr}_x\text{Se}_3$  films with relatively low Cr doping, the ARPES spectra reveal the systematic weakening of the surface states and increasing of the gap amplitude by magnetic impurities [Figs. 4(a)–4(c)], consistent with the previous result [21] and theoretical expectations [27]. When the magnetic doping level is increased to  $x = 0.23$ ,

however, the surface states cannot be observed at all in the ARPES spectrum shown in Fig. 4(d). This suggests that the topological surface states are completely eliminated by strong magnetic doping in the  $x = 0.23$  film, and the system is now a topologically trivial material doped with magnetic impurities, just like conventional DMSs. In fact, the complex temperature evolution of MC in this film shown in Fig. 2(j) is similar to that observed in 2D DMSs such as Mn doped CdSe in the vicinity of metal insulator transition [28]. The mechanism of the localization behavior there is still controversial, but is usually attributed to the large quantum correction to conductivity by the formation of bound magnetic polarons or nanoscale ferromagnetic phases [28]. At low  $T$  the random distribution of these local magnetic clusters causes a dramatic increase of resistivity, which can be strongly reduced when they are aligned by external magnetic field. A WL-like negative magnetoresistance (MR) thus appears and is shown to be closely correlated with the field-induced magnetization. With increasing  $T$ , the field alignment is weakened by thermal fluctuations and the WAL-like positive MR recovers. The strong similarities between the two systems suggest that a similar mechanism involving magnetization-induced WL in competition with SOC-induced WAL may explain the MC behavior in heavily Cr doped  $\text{Bi}_2\text{Se}_3$ .

Therefore, both the ARPES and transport results in the  $x = 0.23 \text{ Bi}_{2-x}\text{Cr}_x\text{Se}_3$  demonstrate, for the first time, the complete suppression of the nontrivial bulk  $Z_2$  topology of TI by a high concentration of magnetic impurities. Although the localization properties in the presence of topological protection and strong magnetic impurities represent a formidable theoretical challenge, we may reach the following phenomenological picture based on our observations. The WAL to WL crossover in  $\text{Bi}_{2-x}\text{Cr}_x\text{Se}_3$  films from  $x = 0$  to  $0.23$  [Fig. 3(c)] is due to the transformation

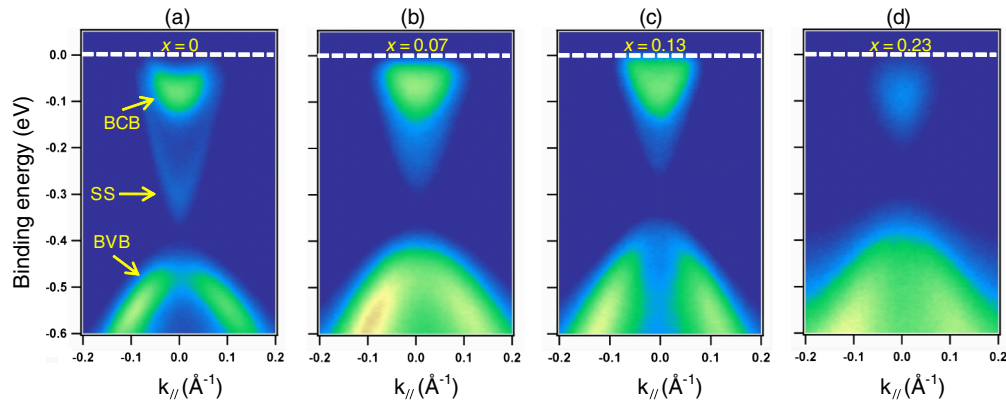


FIG. 4 (color online). (a) ARPES spectrum of pure  $\text{Bi}_2\text{Se}_3$  shows well-resolved Dirac-like surface states. The surface states (SS), bulk conduction band (BCB), and bulk valence band (BVB) are marked by arrows. The  $\Delta \sim 100 \text{ meV}$  gap near the Dirac point is induced by the hybridization between the two surfaces [32]. In the  $x = 0.07$  (b) and  $x = 0.13$  films (c) the surface states become weaker and the gap becomes larger. (d) In the ARPES spectrum of the strongly magnetic  $x = 0.23$  film the surface states totally disappear.

of the system from a TI (with WAL) to a topologically trivial DMS (with WL at low  $T$ ) driven by magnetic impurities. The intermediate doping regime can be described by the interplay between the two phases, where the topological surface states still exist (but weakened) and DMS-like magneto transport starts to emerge. Whether the ground state shows WAL or WL behavior depends on the relative strength of the two competing terms. The exact nature of the interplay, whether it is through microscopic phase coexistence, nanoscale phase separation, competition between different scattering processes or something else, needs to be further investigated.

The WAL to WL crossover problem has also attracted tremendous interest in the studies of graphene, another 2D Dirac fermion system that is closely related to the TIs. It was predicted and experimentally confirmed that such a crossover occurs due to intervalley scattering, which weakens the chiral nature of the Dirac fermions [29,30]. Although the situation in graphene seems to be very different from that in magnetically doped TIs, the underlying physics is similar. The crossover from WAL to WL is driven by certain type of symmetry breaking that suppresses the topological protection. In TIs the WL induced by breaking TRS is opposite to the usual expectation for conventional materials without strong SOC, in which WL dominates when TRS is preserved and diminishes when TRS is broken [31]. This apparent paradox actually reflects the unique physics of the TIs [24,26].

In summary, we observe a complex crossover between WAL and WL in Cr doped  $\text{Bi}_2\text{Se}_3$  TIs, which represents a clear manifestation of the suppression of nontrivial bulk topology by magnetic impurities. The tuning of quantum transport by magnetic doping, temperature, and magnetic field may pave the road for finding the exotic topological effects created by the interplay between topological protection and broken TRS. The realization of both topologically nontrivial spin-momentum locked surface states and topologically trivial DMS may also lead to new spintronic applications.

We thank H.Z. Lu, X.L. Qi, S.Q. Shen, C.S. Tian, Z. Wang, and Z.Y. Weng for helpful discussions. This work was supported by the National Natural Science Foundation of China, the Ministry of Science and Technology of China (grant number 2009CB929400), and the Chinese Academy of Sciences.

\*kehe@aphy.iphy.ac.cn

†yayuwang@tsinghua.edu.cn

- [1] X.L. Qi and S.C. Zhang, *Phys. Today* **63**, 33 (2010).
- [2] J.E. Moore, *Nature (London)* **464**, 194 (2010).
- [3] M.Z. Hasan and C.L. Kane, *Rev. Mod. Phys.* **82**, 3045 (2010).
- [4] D. Hsieh *et al.*, *Nature (London)* **460**, 1101 (2009).
- [5] D. Hsieh *et al.*, *Science* **323**, 919 (2009).
- [6] Y.L. Chen *et al.*, *Science* **325**, 178 (2009).
- [7] P. Roushan *et al.*, *Nature (London)* **460**, 1106 (2009).
- [8] T. Zhang *et al.*, *Phys. Rev. Lett.* **103**, 266803 (2009).
- [9] Z. Alpichshev *et al.*, *Phys. Rev. Lett.* **104**, 016401 (2010).
- [10] J. Chen *et al.*, *Phys. Rev. Lett.* **105**, 176602 (2010).
- [11] M.H. Liu *et al.*, *Phys. Rev. B* **83**, 165440 (2011).
- [12] H.T. He *et al.*, *Phys. Rev. Lett.* **106**, 166805 (2011).
- [13] J.G. Checkelsky *et al.*, *Phys. Rev. Lett.* **106**, 196801 (2011).
- [14] X.L. Qi, T.L. Hughes, and S.C. Zhang, *Phys. Rev. B* **78**, 195424 (2008).
- [15] X.L. Qi *et al.*, *Science* **323**, 1184 (2009).
- [16] L. Fu and C.L. Kane, *Phys. Rev. Lett.* **102**, 216403 (2009).
- [17] W.K. Tse and A.H. MacDonald, *Phys. Rev. Lett.* **105**, 057401 (2010).
- [18] R. Yu *et al.*, *Science* **329**, 61 (2010).
- [19] Y. Xia *et al.*, *Nature Phys.* **5**, 398 (2009).
- [20] H.J. Zhang *et al.*, *Nature Phys.* **5**, 438 (2009).
- [21] Y.L. Chen, *Science* **329**, 659 (2010).
- [22] L.A. Wray *et al.*, *Nature Phys.* **7**, 32 (2010).
- [23] See Supplementary Material at <http://link.aps.org/supplemental/10.1103/PhysRevLett.108.036805> for details on the effect of film thickness on the transport properties and the analysis of the MC curves using the HLN formula.
- [24] K. Nomura, M. Koshino, and S. Ryu, *Phys. Rev. Lett.* **99**, 146806 (2007).
- [25] S. Hikami, A.I. Larkin, and Y. Nagaoka, *Prog. Theor. Phys.* **63**, 707 (1980).
- [26] H.Z. Lu, J.R. Shi, and S.Q. Shen, *Phys. Rev. Lett.* **107**, 076801 (2011).
- [27] Q. Liu *et al.*, *Phys. Rev. Lett.* **102**, 156603 (2009).
- [28] T. Dietl, *J. Phys. Soc. Jpn.* **77**, 031005 (2008).
- [29] E. McCann *et al.*, *Phys. Rev. Lett.* **97**, 146805 (2006).
- [30] F.V. Tikhonenko *et al.*, *Phys. Rev. Lett.* **103**, 226801 (2009).
- [31] P.A. Lee and T.V. Ramakrishnan, *Rev. Mod. Phys.* **57**, 287 (1985).
- [32] Y. Zhang *et al.*, *Nature Phys.* **6**, 584 (2010).